Original Article

Cardiac magnetic resonance imaging detection of intramyocardial hemorrhage in patients with ST-elevated myocardial infarction: comparison between susceptibility-weighted imaging and T1/T2 mapping techniques

Jinyang Wen[1], Jinhan Qiao[1], Yuanyuan Tang[1], Yun Zhao[1], Zhaoxia Yang[1], Luyun Wang[2], Xinwei Tao[3], Xiaoyue Zhou[4], Liming Xia[1], Dazhong Tang[1#], Lu Huang[1#]

[1]Department of Radiology, Tongji Hospital, Tongji Medical College, Huazhong University of Science and Technology, Wuhan, China; [2]Division of Cardiology, Department of Internal Medicine, Hubei Key Laboratory of Genetics and Molecular Mechanism of Cardiological Disorders, Tongji Medical College, Huazhong University of Science and Technology, Wuhan, China; [3]Bayer Healthcare, Shanghai, China; [4]MR Collaboration, Siemens Healthineers Ltd., Shanghai, China

Contributions: (I) Conception and design: J Wen, J Qiao; (II) Administrative support: L Huang, D Tang, X Tao, X Zhou, L Xia; (III) Provision of study materials or patients: J Qiao, D Tang, L Wang; (IV) Collection and assembly of data: J Wen, J Qiao; (V) Data analysis and interpretation: J Wen, Z Yang; (VI) Manuscript writing: All authors; (VII) Final approval of manuscript: All authors.

[#]These authors contributed equally to this work.

Correspondence to: Lu Huang, MD, PhD; Dazhong Tang, MM. Department of Radiology, Tongji Hospital, Tongji Medical College, Huazhong University of Science and Technology, 1095 Jiefang Avenue, Wuhan 430030, China. Email: tj_lhuang@hust.edu.cn; tangdazhong2004@163.com.

Background: Susceptibility-weighted imaging (SWI) and T1/T2 mapping can be used to detect reperfusion intramyocardial hemorrhage (IMH) in ST-segment elevation myocardial infarction (STEMI) patients. However, the sensitivity and accuracy of the SWI and T1/T2 mapping sequences were not systematically compared. The study aimed to evaluate image quality and diagnostic performance of SWI in patients with IMH, compared with T1/T2 mapping.

Methods: A prospective study was conducted on consecutive acute STEMI patients who were recruited from January to July 2022. Within 2–6 days after reperfusion treatment, all patients underwent a 3T cardiac magnetic resonance (CMR) examination, including T2-weighted short-tau inversion recovery (T2W-STIR), T1/T2 mapping, and SWI. A total of 36 patients [age, 56.50±17.25 years; males, 83.33% (30/36)] were enrolled. The relative infarct-remote myocardium signal intensity ratio (SIinfarct-remote) and contrast-to-noise ratio (CNR) were calculated for each patient on T1/T2 mapping and SWI, and the difference between relative signal intensity-to-noise ratio (rSNR) in the IMH (rSNRIMH) was measured for IMH patients on T1/T2 mapping and SWI. SIinfarct-remote, CNR, and rSNRIMH were compared among the three sequences. Receiver operating characteristic (ROC) analyses were used to evaluate the diagnostic performance of three sequences by SIinfarct-remote and visual assessment.

Results: A total of 26 (72.22%) patients had IMH. Quantitatively, the SIinfarct-remote of three sequences had excellent diagnostic performance for detecting IMH [SWI area under the curve (AUC) =1.000, 95% confidence interval (CI): 1.000–1.000 *vs.* T1 mapping AUC =0.954, 95% CI: 0.885–1.000 *vs.* T2 mapping AUC =0.985, 95% CI: 0.955–1.000; SWI *vs.* T1 mapping, P=0.300; SWI *vs.* T2 mapping, P=0.188; T1 mapping *vs.* T2 mapping, P=0.302). Qualitatively, three sequences had similar performance on detecting IMH (SWI AUC =0.895, 95% CI: 0.784–1.000; T1 mapping AUC =0.835, 95% CI: 0.711–0.958; and T2 mapping AUC =0.855, 95% CI: 0.735–0.974; SWI *vs.* T1 mapping, P=0.172; SWI *vs.* T2 mapping, P=0.317; T1 mapping *vs.* T2 mapping, P=0.710). The rSNRIMH was highest in T1 mapping, followed by T2

mapping and SWI, but SWI had the highest CNR.

Conclusions: SWI, as well as T1/T2 mapping, is a feasible and accurate approach for clinical diagnosis of IMH with excellent performance.

Keywords: Susceptibility-weighted imaging (SWI); T1 mapping; T2 mapping; intramyocardial hemorrhage (IMH); cardiac magnetic resonance (CMR)

Submitted Apr 28, 2023. Accepted for publication Nov 02, 2023. Published online Nov 28, 2023.
doi: 10.21037/qims-23-591
View this article at: https://dx.doi.org/10.21037/qims-23-591

Introduction

Percutaneous coronary intervention (PCI) has been established as a preferred treatment for acute ST-segment elevation myocardial infarction (STEMI) patients to restore the occluded coronary artery blood flow as quickly as possible (1). Nevertheless, reperfusion injury may occur during this process, aggravating the damage to cardiomyocytes and resulting in microvascular obstruction (MO). Coronary MO underlies intramyocardial hemorrhage (IMH), leading to capillary endothelial cell rupture and the leakage of red blood cells from vessels (2). As a result, IMH may enlarge myocardial infarction (MI) size (3). In addition, IMH is closely related to left ventricular remodeling and adverse cardiovascular events (4-7). Hence, IMH detection after reperfusion treatment in STEMI patients is vitally important.

Currently, cardiac magnetic resonance (CMR) is the gold standard for detecting IMH noninvasively (2,8,9), T2-weighted short-tau inversion recovery (T2W-STIR) imaging has been allowed for the visualization of IMH within the infarction, which was defined as a characteristic hypointense core in the hyperintense edema region (10-12). Although T2-weighted is the common sequence for detecting iron in the heart, the image quality from T2W-STIR may be degraded due to increased phase differences among tissues at high field strength (13). Further, T2W-STIR is less sensitive to hemorrhagic and calcified lesions compared with iron-sensitive sequences, such as T2* (14). Susceptibility-weighted imaging (SWI) is a routine examination used to detect microhemorrhage and microvascular malformations; it relies on the paramagnetic effect of deoxyhemoglobin degradation products (15,16), and this effect may be more prominent at high field strength. SWI is also an accurate and reproducible way detect reperfusion IMH in STEMI patients at 1.5 T (17) and offers shorter breath hold times than T2-weighted at 3.0 T (18). Besides, SWI allows semi-quantitative analysis due to its sensitivity to small volume hemorrhage detection (18). T1 mapping and T2 mapping have also been used to determine IMH (9,14) in patients and animals. IMH presents as a hypointense core on the native T1/T2 map, which could allow for the quantitative evaluation of IMH and serves as an alternative when T2* images cannot be easily acquired (9,14). However, the sensitivity and accuracy of the SWI and T1/T2 mapping sequences in the focal iron lesion have not been systematically compared in IMH patients, particularly at 3.0 T.

This study aimed to compare the diagnostic performance of SWI with T1/T2 mapping in detecting IMH in STEMI patients. Furthermore, the study aimed to evaluate the image quality and feasibility of SWI, using T2-weighted imaging (T2WI) as a reference standard. We present this article in accordance with the STARD reporting checklist (available at https://qims.amegroups.com/article/view/10.21037/qims-23-591/rc).

Methods

Study population

This prospective study was approved by the Ethics Committee of Tongji Hospital (No. [2019] S1184), and all participants provided informed consent. The study was conducted in accordance with the Declaration of Helsinki (as revised in 2013). A total of 71 STEMI patients treated by PCI within 12 hours of onset who were referred to our department for CMR were consecutively recruited between January and July 2022. STEMI was diagnosed following the current guidelines (1,19). The exclusion criteria were as follows: (I) previous MI; (II) contraindications to CMR, such as glomerular filtration rate <30 mL/min, permanent pacemakers, and claustrophobia; and (III) CMR images unable to be evaluated due to severe artifacts. All the patients' clinical data were obtained from the electronic

Table 1 Magnetic resonance scanning sequence and specific parameters

Parameters	bSSFP cine	T2W-STIR	T1 mapping	T2 mapping	SWI	LGE
TR (ms)	3.1	Two R-R intervals	2.5	3.3	9.0	3.1
TE (ms)	1.4	92	1.2	1.35	6.27	1.2
Flip angle (degree)	55	90	35	15	15	55
FOV (mm^2)	360×360	360×360	360×360	360×360	340×340	360×360
Slice thickness (mm)	8	8	8	8	2.5	8
Voxel size (mm^3)	1.9×1.9×8.0	0.7×0.7×8.0	1.4×1.4×8.0	1.9×1.9×8.0	0.8×0.8×2.5	1.5×1.5×8.0

bSSFP, balanced steady-state free precession; T2W-STIR, T2-weighted short-tau inversion recovery; SWI, susceptibility-weighted imaging; LGE, late gadolinium enhancement; TR, repetition time; ms, milliseconds; TE, echo time; FOV, field of view.

medical record system. We used SPSS software (IBM Corp., Armonk, NY, USA) to calculate the sample size. Based on the 20 patients' results of our pre-experiment, the mean of $T1_{infarct\text{-}remote}$ in the two groups (IMH and non-IMH) were set 0.8 and 1.3, respectively, and standard deviation (SD) was 0.38. The calculated sample size of the two groups were 20 and 10, the total sample size was 30 with 90% power and a type I error frequency of 5%. So, the final sample size was sufficient.

CMR image acquisition

All patients underwent a CMR examination within 7 days on a 3-T scanner (MAGNETOM Skyra, Siemens Healthcare, Erlangen, Germany) with an 18-channel phase-array body coil combined with 12-channel spine coil and electrocardiograph (ECG) gating. The CMR protocol included short-axis cine, late gadolinium enhancement (LGE), native T1 mapping, T2 mapping, T2W-STIR, and three-dimensional (3D) SWI. In addition, all the short-axis slices of native T1 mapping, T2 mapping, and T2W-STIR were matched with the position of the cine. The exact protocol was performed: first unenhanced balanced steady-state free precession (bSSFP) cine sequences, followed by T2W-STIR, native T1 mapping, T2 mapping, then SWI sequence, and finally LGE sequence. The average scanning time was 50±5 minutes, the imaging parameter are summarized in *Table 1*.

The short-axis cine adopted bSSFP sequence, covering the left ventricle (LV) from base to apex. T2WI adopted a dark-blood T2W-STIR sequence with ECG gating. The native T1 mapping adopted the modified Look-locker inversion recovery (MOLLI) sequence with the 5b (3b) 3b (b for heartbeat) acquisition protocol (20). For one-slice imaging, T2-prepared single-shot sequence with 3 T2 preparation duration: 0, 30, and 55 ms. A recovery duration of 3b was set in between the T2 preparation pulses to wait for the magnetization to be fully recovered. In addition, SWI used a 3D gradient echo sequence under breath-holding (required 15–23 seconds), and also covered the whole LV. The direction of the phase coding was set according to the direction of contractile movement of the infarcted myocardium in each patient. Proper adjustment of the phase encoding direction could reduce the artifact caused by respiration and the heartbeat. The decreased movement of the infarcted myocardium can also reduce motion artifacts. A set of four images [magnitude, phase, maximum intensity projection (MIP), and SWI] were generated in line. LGE image acquisition was performed 10–15 minutes after gadobutrol (Gadovist; Bayer Schering Pharma AG, Leverkusen, Germany) injection of 0.1 mmol/kg and a 20 mL normal saline rinse. Then, a two-dimensional (2D) phase-sensitive inversion recovery sequence (PSIR) was used to obtain the LGE images, and the inversion time was 220 to 350 ms. All the above scans were conducted under breath holding to eliminate respiratory motion artifacts.

CMR imaging analysis

CMR imaging was analyzed by CVI[42] software version 5.12.1 (Circle Cardiovascular Imaging, Calgary, AB, Canada). LV endocardial and epicardial contours on the short-axis cine images were automatically tracked and manual corrections were made if needed. The LV function parameters, including LV end-diastolic volume (LVEDV), LV end-systolic volumes (LVESV), LV ejection fraction (LVEF), cardiac index, and LV mass, were evaluated and

standardized by body surface area (BSA).

MI size was calculated by mass (grams), standardized by BSA, and a percentage of the LV mass (%LV) using a signal intensity (SI) threshold of five SDs above the remote myocardium (normal myocardium distant from the infarct zone) in the LGE images (21). Furthermore, IMH was defined as a hypointense core in the hyperintense edema region on the T2W-STIR, corresponding to a lack of enhancement on the LGE images, as previous studies described (10,17,18). IMH presented as hypointense and hyperintense on the SW and phase images, respectively, corresponding to the T2W-STIR hypointense core (22).

On the T1/T2 mapping and SWI images, regions of interest (ROIs) were manually drawn in hypointense core within the infarcted zone, which the SI defined as $T1_{infarct}$, $T2_{infarct}$, and $SWI_{infarct}$, and the SI of the remote myocardium defined as $T1_{remote}$, $T2_{remote}$, and SWI_{remote}. When no hypointense core was found in images, the ROI was drawn in the area of infarction. The same ROIs were used through different imaging sequences. The SDs of these ROIs were also recorded. The relative infarct-remote myocardium SI ratio ($SI_{infarct\text{-}remote}$) was calculated for each patient through three imaging sequences to compare the performance of detecting IMH. Similarly, image quality was assessed by relative SI-to-noise ratio (rSNR) within IMH area and contrast-to-noise ratio (CNR) between the core area of infarction and remote area; the measurement of SNR/CNR is shown in Figure S1. rSNR of the IMH area was defined as $rSNR_{IMH}$. The $SI_{infarct\text{-}remote}$, rSNR, and CNR were calculated with the following formula (17,18):

$$T1_{infarct\text{-}remote} = \frac{T1_{infarct}}{T1_{remote}} \quad [1]$$

$$T2_{infarct\text{-}remote} = \frac{T2_{infarct}}{T2_{remote}} \quad [2]$$

$$SWI_{infarct\text{-}remote} = \frac{SWI_{infarct}}{SWI_{remote}} \quad [3]$$

$$rSNR_{IMH} = 0.655 * \frac{SI_{infarct}}{SD} \quad [4]$$

$$CNR = \frac{\left|SI_{remote} - SI_{infarct}\right|}{SD\left(SI_{remote}\right)} \quad [5]$$

SWI, T1 mapping, and T2 mapping images were independently evaluated for the presence of IMH and access SI by two blinded reviewers (J.W. and Z.Y., each with more than 5 years of CMR experience). Any disagreement on the presence of IMH between reviewers was resolved by a consensus read. After 2 weeks, one of the radiologists repeated the same assessment procedure.

Statistical analysis

The software IBM SPSS 23.0 and R version 4.1.2 (RStudio, Boston, MA, USA) were used to analyze the data. Normal distributions were assessed using Kolmogorov-Smirnov's test. Normally distributed variables were expressed as means ± SD, whereas non-normally distributed variables are reported as median with interquartile ranges. In addition, a paired or unpaired *t*-test was used for normally distributed data, and the Mann-Whitney *U* test was used for skewed data. A paired *t*-test was used for pairwise comparison and statistical significance was considered when $P<0.05/3$ to control for error type I. Categorical data were expressed as frequencies (percentages) and compared with Fisher's exact test. The diagnostic performance of SWI and T1/T2 mapping to detect IMH on the three sequences was evaluated qualitatively and quantitively using receiver operating characteristic (ROC) analyses and was compared using the Delong test (23). Finally, inter- and intra-observer reproducibility were evaluated by the intraclass correlation coefficient (ICC) for continuous measurements and Cohen's kappa statistic for the binary assessment. Statistical significance was indicated by two-sided tests of $P<0.05$.

Results

Image scanning and imaging quality

A total of 41 patients had undergone the whole CMR protocol scanning. T2W-STIR were not available in 12% (5/41) of the patients due to obvious artifacts but the remaining 36 patients' corresponding SWI, T1, and T2 maps were interpretable. The flow chart of the study enrollment is presented in *Figure 1*. In particular, all the SWI images could be used to evaluate IMH in the STEMI patients with breath-holding. *Figure 2* shows several representative cases with SWI images of different qualities used to detect IMH.

Clinical characteristics of the STEMI patients

A total of 36 STEMI patients [age, 56.50 (17.25) years; 30 males (83.33%)] were enrolled in our study. A total of 26 (72.22%) patients had IMH with T2W-STIR images as a reference. The proportion of patients with dyslipidemia in the IMH group was markedly higher than that in the non-IMH group. IMH group had higher peak high-sensitivity cardiac troponin I (hs-cTnI) level compared with the non-IMH group. Further clinical characteristics details are

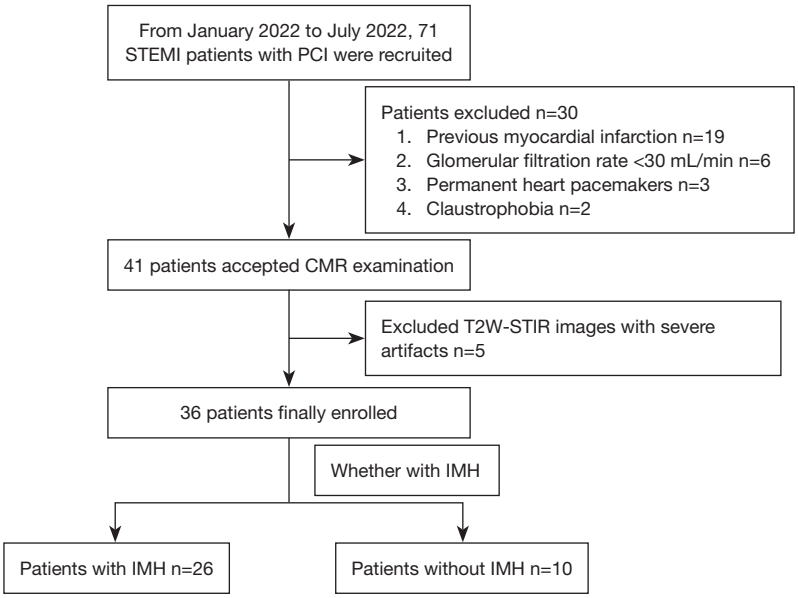

Figure 1 Flowchart of study population enrollment. STEMI, ST-segment elevation myocardial infarction; PCI, percutaneous coronary intervention; CMR, cardiac magnetic resonance; T2W-STIR, T2-weighted short-tau inversion recovery; IMH, intramyocardial hemorrhage.

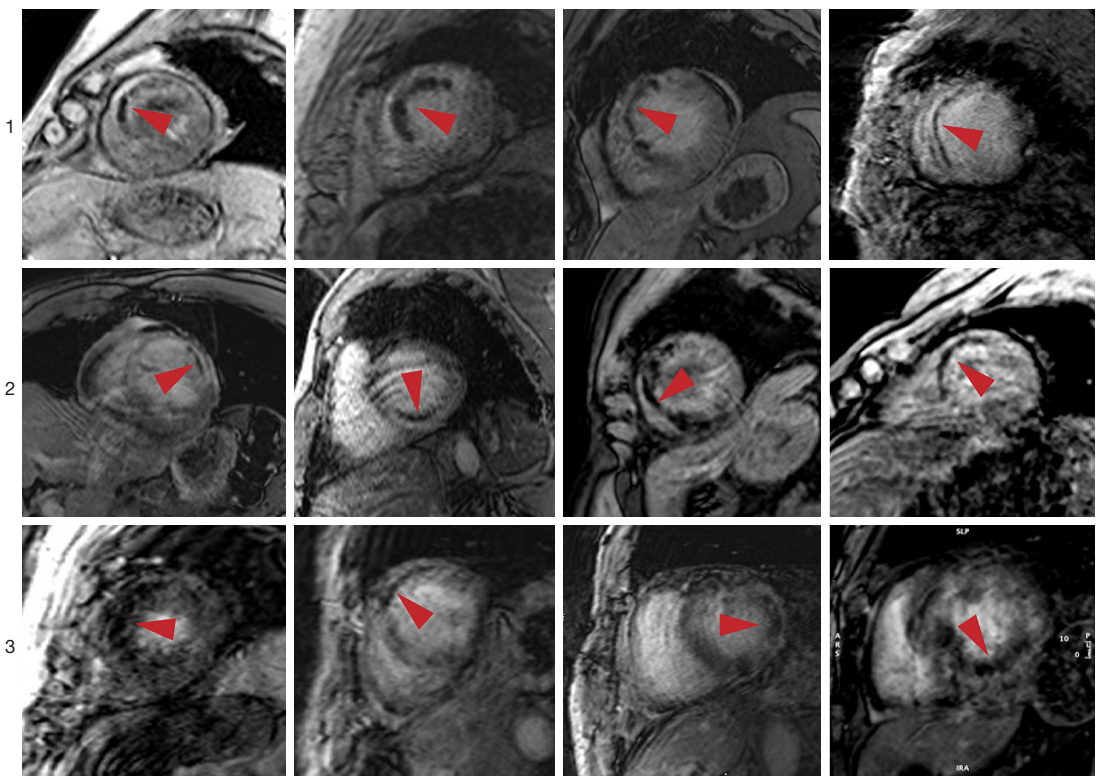

Figure 2 Several representative cases with SWI images of different quality to detect IMH (red arrows). 1: excellent image quality; 2: minor artifacts outside of the IMH; 3: artifacts in IMH but analysis possible. SWI, susceptibility-weighted imaging; IMH, intramyocardial hemorrhage.

Table 2 Clinical characteristics of STEMI patients

Characteristics	STEMI patients (n=36)	IMH (n=26)	Non-IMH (n=10)	P value
Male	30 (83.33)	21 (80.77)	9 (90.00)	0.655
Age (years)	56.50 (17.25)	56 (20.25)	64 (13.75)	0.080
BMI (kg/m^2)	25.63±2.99	25.82±2.96	25.13±3.17	0.544
Hypertension	18 (50.00)	12 (46.15)	6 (60.00)	0.711
Smoking	22 (61.11)	14 (53.85)	8 (80.00)	0.255
Diabetes mellitus	12 (33.33)	9 (34.62)	3 (30.00)	>0.99
Dyslipidemia	22 (61.11)	19 (73.08)	3 (30.00)	0.026*
Peak hs-cTnI (ng/mL)	35,817.90 [38,210.35]	48,813.60 [33,384.53]	11,855.80 [15,077.15]	0.009*
Peak NT-proBNP (pg/mL)	547.50 [1,344.50]	577 [1,418.75]	437 [1,170.50]	0.689
PCI onset to CMR time (days)	4 [2]	4 [3]	4 [2]	0.493
Pre-PCI TIMI flow grade				0.570
0	16 (44.44)	13 (50.00)	3 (30.00)	
1	9 (25.00)	5 (19.23)	4 (40.00)	
2	10 (27.78)	7 (26.92)	3 (30.00)	
3	1 (2.78)	1 (3.85)	0	
Post-PCI TIMI flow grade				0.071
0	0	0	0	
1	0	0	0	
2	2 (5.56)	0	2 (20.00)	
3	34 (94.44)	26 (100.00)	8 (80.00)	
Infarct artery				>0.99
LAD	22 (61.11)	16 (61.54)	6 (60.00)	
LCX	5 (13.89)	4 (15.38)	1 (10.00)	
RCA	9 (25.00)	6 (23.08)	3 (30.00)	

Values are n (%), mean ± SD, or median [interquartile range]. P value represents IMH group vs. non-IMH group. *, P value <0.05 are statistically significant. STEMI, ST-segment elevation myocardial infarction; IMH, intramyocardial hemorrhage; BMI, body mass index; hs-cTnI, high-sensitivity cardiac troponin I; NT-proBNP, N-terminal pro-brain natriuretic peptide; PCI, percutaneous coronary intervention; CMR, cardiac magnetic resonance; TIMI, thrombolysis in myocardial infarction; LAD, left anterior descending artery; LCX, left circumflex artery; RCA, right coronary artery; SD, standard deviation.

shown in *Table 2*.

CMR parameter differences between the IMH and non-IMH groups

On the T1/T2 map and SWI images, a hypointense core was found in 61.11% (22/36), 69.44% (25/36), and 72.22% (26/36), of the patients, respectively. A total of 26 patients with available T2W-STIR had IMH. A representative case of IMH is shown in *Figure 3*.

A larger infarct size was found in the IMH group compared to the non-IMH group [27.87% (7.55%) *vs.* 15.00% (5.95%), P=0.004]. Furthermore, in the IMH group, the LVESVI was significantly dilated, and the LVEF was significantly impaired. In the patients with IMH, $T1_{infarct}$ was lower than that of the non-IMH patients (1,054.70±156.10 *vs.* 1,472.00±109.38 ms, P<0.001), $T1_{remote}$ was not statistically different between the IMH and non-

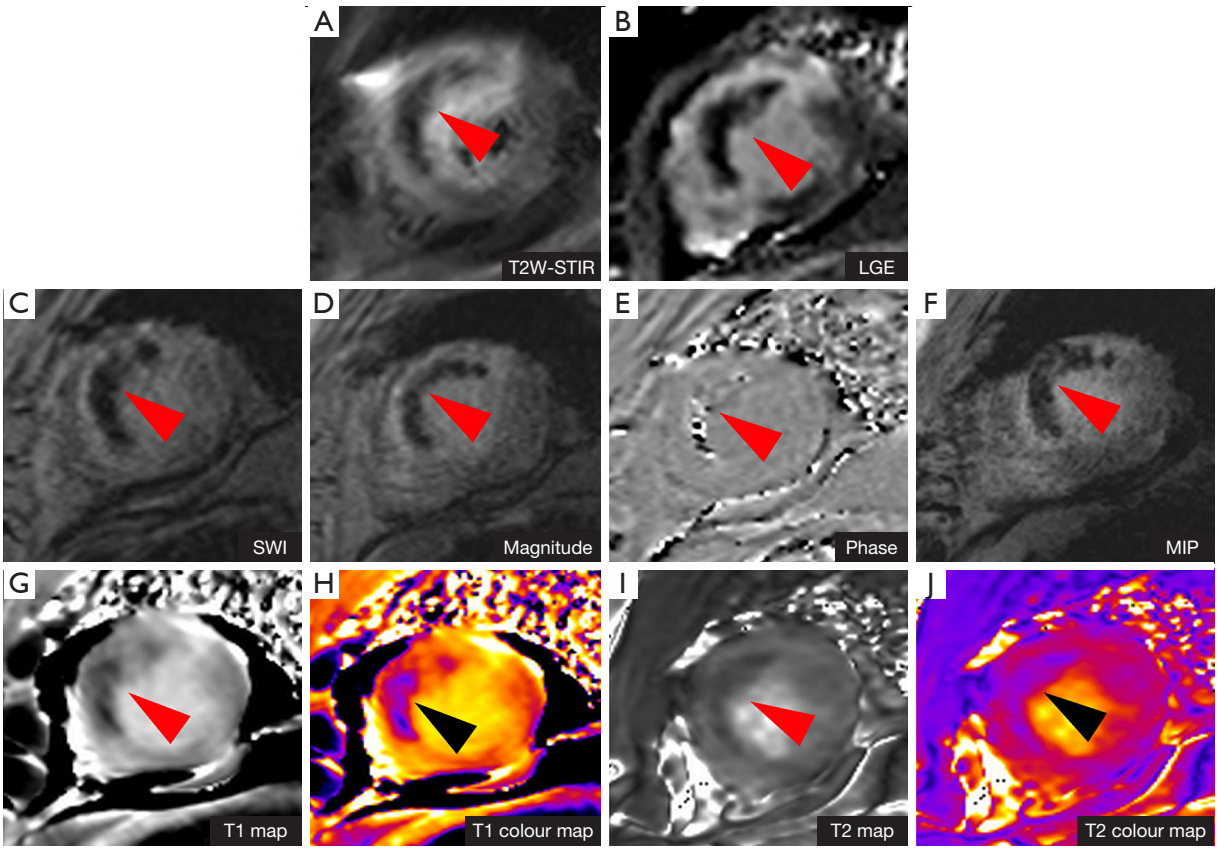

Figure 3 CMR images of a STEMI patient with IMH presentation after receiving PCI therapy. IMH is presented as a hypointense core within a hyperintense area in the T2W-STIR image (A) corresponding to the infarcted area in the LGE images (B). The same hypointense and hyperintense areas are shown in the SWI (C), Magnitude (D), Phase (E), MIP (F), T1 map (G,H), and T2 map (I,J) images with the red or black arrows indicating IMH within myocardial infarction. T2W-STIR, T2-weighted short-tau inversion recovery; LGE, late gadolinium enhancement; SWI, susceptibility-weighted imaging; MIP, maximum intensity projection; CMR, cardiac magnetic resonance; STEMI, ST-segment elevation myocardial infarction; IMH, intramyocardial hemorrhage; PCI, percutaneous coronary intervention.

IMH groups (1,256.50±61.54 *vs.* 1,249.00±91.88 ms, P=0.203), which was similar to the performance of $T2_{infarct}$ and $T2_{remote}$ value between the two groups ($T2_{infarct}$: 30.28±5.61 *vs.* 54.16±8.32 ms, P<0.001; $T2_{remote}$: 40.69±5.36 *vs.* 42.71±6.69 ms, P=0.352). The IMH group had the lower $SWI_{infarct}$ than non-IMH group, but there was no statistical difference in SWI_{remote} ($SWI_{infarct}$: 34.99±18.26 *vs.* 106.19±69.69 ms, P<0.001; SWI_{remote}: 84.26±30.24 *vs.* 61.16±27.47 ms, P=0.076). Further CMR findings are shown in *Table 3*.

The $SI_{infarct}$, SI_{remote}, and $SI_{infarct-remote}$ on T1 mapping, T2 mapping, and SWI

$SI_{infarct}$, SI_{remote}, and $SI_{infarct-remote}$ on the three types of images in the IMH group and non-IMH group are shown in *Figure 4* and *Table 3*. In the IMH group, $SI_{infarct}$ was lower than SI_{remote} on T1 mapping, T2 mapping, and SWI. In the non-IMH group, $SI_{infarct}$ was higher than SI_{remote} on T1 mapping and T2 mapping, but there was no statistical significance between $SI_{infarct}$ and SI_{remote} on SWI images. In addition, $SWI_{infarct-remote}$ in the IMH group was significantly lower than that (0.41±0.13 *vs.* 1.55±0.49 ms, P<0.001) in the non-IMH group, consistent with the results on the T1/T2 map images.

ROC comparison of the three imaging sequences for detecting IMH

The quantitative parameters were analyzed by $T1_{remote-core}$, $T2_{remote-core}$, and $SWI_{remote-core}$ in ROC curve analysis. Visual assessment was used for the qualitative way ROC curve

Table 3 CMR parameters of the IMH and non-IMH groups among the STEMI patients

Characteristics	IMH (n=26)	Non-IMH (n=10)	P value
LVEDV per BSA increase [/(mL·m^2)]	79.60 (18.90)	75.71 (22.74)	0.373
LVESV per BSA increase [/(mL·m^2)]	51.22 (19.71)	38.43 (17.92)	0.023*
LVEF (%)	32.3±10.4	47.6±13.0	<0.001*
CI [L/(min·m^2)]	1.97 (0.58)	2.34 (0.87)	0.069
LV mass per BSA increase (g/m^2)	74.51±18.90	73.87±24.94	0.934
Infarct mass (g)	38.89 (18.48)	14.34 (8.00)	<0.001*
Infarct mass of LV (%)	27.87 (7.55)	15.00 (5.95)	0.004*
$T1_{infarct}$ (ms)	1,054.70±156.10	1,472.00±109.38	<0.001*
$T1_{remote}$ (ms)	1,256.50±61.54	1,249.00±91.88	0.203
$T2_{infarct}$ (ms)	30.28±5.61	54.16±8.32	<0.001*
$T2_{remote}$ (ms)	40.69±5.36	42.71±6.69	0.352
$SWI_{infarct}$ (ms)	34.99±18.26	106.19±69.69	<0.001*
SWI_{remote} (ms)	84.26±30.24	61.16±27.47	0.076
$T1_{infarct-remote}$ (ms)	0.84±0.12	1.19±0.13	<0.001*
$T2_{infarct-remote}$ (ms)	0.75±0.14	1.28±0.22	<0.001*
$SWI_{infarct-remote}$ (ms)	0.41±0.13	1.55±0.49	<0.001*

Values are median (interquartile range) or mean ± SD. *, P value <0.05 are statistically significant. CMR, cardiac magnetic resonance; IMH, intramyocardial hemorrhage; STEMI, ST-segment elevation myocardial infarction; LVEDV, left ventricular end-diastolic volume; BSA, body surface area; LVESV, left ventricular end-systolic volume; LVEF, left ventricular ejection fraction; CI, cardiac index; LV, left ventricular; ms, milliseconds; SWI, susceptibility-weighted imaging; SD, standard deviation.

analysis. Both quantitatively and qualitatively, the three imaging sequences demonstrated an excellent performance [all areas under the curve (AUCs) exceeded 0.9, *Table 4*]. The Delong test showed no statistical difference (P>0.05 for all). Also, the cross-tabulation results of diagnostic results of the reference standard and three imaging sequences are shown in Table S1.

Comparison of image quality among the three imaging sequences in the IMH patients

The highest $rSNR_{IMH}$ was T1 mapping (20.84±8.58), followed by T2 mapping (10.35±4.78) and SWI (5.63±4.94) (P<0.016 for all). In contrast, the CNR was the highest on SWI among three imaging sequences, the CNR of T2 mapping was the lowest (*Figure 5*) (SWI *vs.* T1 mapping *vs.* T2 mapping: 9.84±3.94 *vs.* 6.99±4.21 *vs.* 4.68±2.25, P<0.016 for all).

Inter- and intra-observer variability

All the $SI_{infarct-remote}$ values ($T1_{remote-infarct}$, $T2_{remote-infarct}$, and $SWI_{remote-infarct}$) exhibited excellent (ICC >0.80) intraobserver and interobserver consistency. The ICCs and Cohen's kappa with 95% confidence intervals (CIs) are summarized in Table S2.

Discussion

The results of our study demonstrate the following major findings: (I) SWI, as well as T1 mapping and T2 mapping sequences could feasibly detect IMH after reperfusion therapy in acute STEMI patients with excellent performance and high reproducibility; (II) the hypointense core on SWI at 3.0-T CMR could be used to confirm the presence of IMH with excellent tissue contrast.

CMR examination is essential for IMH detection in STEMI patients following reperfusion treatment, since

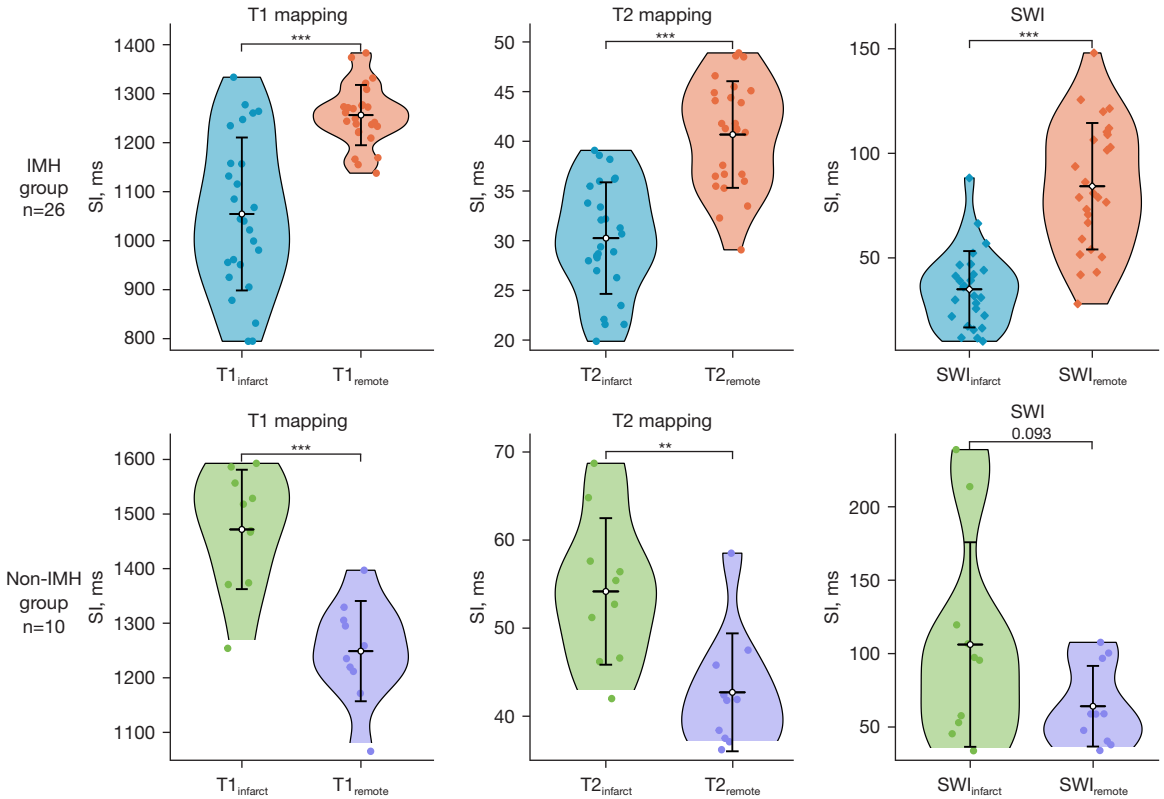

Figure 4 SI values for the infarcted myocardium and remote myocardium from the three MRI sequences. **, P<0.01; ***, P<0.001. IMH, intramyocardial hemorrhage; SI, signal intensity; ms, milliseconds; SWI, susceptibility-weighted imaging.

Table 4 Diagnostic performance of the three imaging sequences to detect IMH

Sequences	Cut-off value	AUC (95% CI)	Sensitivity (%)	Specificity (%)
$SI_{infarct\text{-}remote}$				
$T1_{infarct\text{-}remote}$	1.100	0.954 (0.885–1.000)	80	100
$T2_{infarct\text{-}remote}$	0.893	0.985 (0.955–1.000)	100	88
$SWI_{infarct\text{-}remote}$	0.891	1.000 (1.000–1.000)	100	100
Visualization				
T1 mapping	–	0.835 (0.711–0.958)	91	76
T2 mapping	–	0.855 (0.735–0.974)	91	80
SWI	–	0.895 (0.784–1.000)	91	88

IMH, intramyocardial hemorrhage; AUC, area under the curve; CI, confidence interval; SI, signal intensity; SWI, susceptibility-weighted imaging.

IMH has been linked to adverse LV remodeling, arrhythmic risk, and major cardiovascular events (2,4). Due to the lack of effective *in vivo* assessment technology, clinical research in detecting IMH after AMI has lagged. In 2006, van den Bos *et al.* (12) first applied the porcine ischemia-reperfusion model to confirm the rationality of using T2* to assess IMH, and T2* mapping is currently recommended as a robust method to detect IMH (4,10,13,18,24), but they are more suitable for applying for 1.5 T field strength (25). In recent studies, T1 and T2 mapping performed well

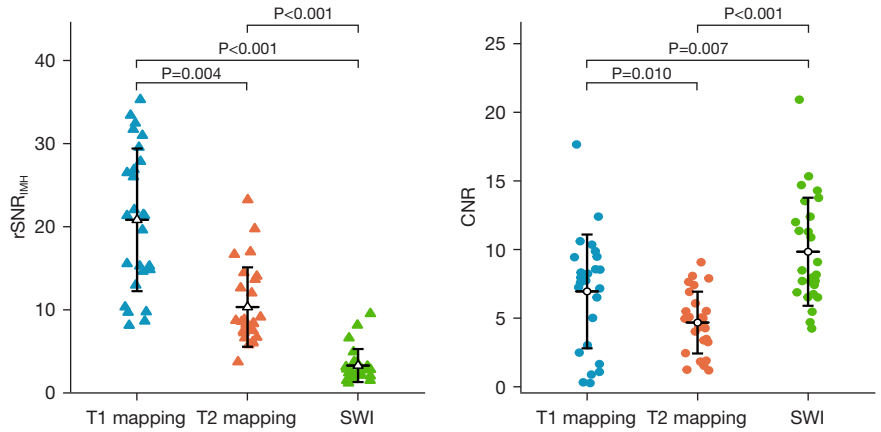

Figure 5 The comparison of $rSNR_{IMH}$ and CNR on three MRI sequences. $rSNR_{IMH}$, relative signal intensity-to-noise ratios within IMH area; IMH, intramyocardial hemorrhage; SWI, susceptibility-weighted imaging; CNR, contrast-to-noise ratio; MRI, magnetic resonance imaging.

in quantitative IMH detection in acute STEMI patients after reperfusion (14,26) and even in rats at 7 T MR (9). The characteristic low-signal infarct core in IMH on T2* imaging was closely related to the paramagnetic effect of deoxyhemoglobin degradation products (27). Hence, the same principle enables IMH to present as hypointense on SWI images. SWI performance has been compared to T2 and T2* imaging for the detection of IMH. Kidambi *et al.* (18) and Blondiaux *et al.* (28) found that SWI could accurately identify IMH after acute MI in both patients and animals. One of the strengths of our study was that the diagnostic performance of SWI and T1/T2 mapping to detect IMH in STEMI patients at 3 T MR was directly compared, a factor that has not previously been studied.

In our study, $T1_{infarct}$ and $T2_{infarct}$ in the IMH group were lower than that in the non-IMH group, which was consistent with previous research (14); it is not surprising that hemorrhage reduces the signal to the myocardium. Similarly, the performance on SWI sequence was no exception. Meantime, in the SI value comparison between the infarcted myocardium and remote myocardium, we found that $SI_{infarct}$ was lower than SI_{remote} in the IMH group on T1/T2 mapping, but $SI_{infarct}$ was all higher than SI_{remote} in the non-IMH group. A reasonable explanation may be that edema increases myocardial signals. On SWI images, the IMH group also had the lower $SI_{infarct}$ than SI_{remote}, but there was no difference between $SI_{infarct}$ and SI_{remote} in the non-IMH group. We assume that edema does not affect myocardial signal in SWI imaging. These factors make it possible to detect hemorrhage in practice.

Since the relativity of SI was not suitable for quantifying IMH tissue characteristics, we chose the SI ratio of the infarct myocardium and remote normal myocardium to achieve IMH detection. In our study, $SI_{infarct\text{-}remote}$ presented significantly different between the IMH and non-IMH groups on the three sequences. Goldfarb *et al.* found that SWI technique can be used to visually assess IMH due to a phase decrease (22). Another study found that decreased T1/T2 value of infarcted zone can also be used to determine the presence of IMH (14). The above findings explain why the signal in the IMH area was lower than that in the normal area. In our study, we found that the $SI_{infarct\text{-}remote}$ ($T1_{infarct\text{-}remote}$, $T2_{infarct\text{-}remote}$, and $SWI_{infarct\text{-}remote}$) value in IMH group was lower, which was consistent with previous studies and indicated that the hypointense core of the infarcted region was distinguishable from normal myocardium. In addition, we extended the semiquantitative measurement of IMH to SWI images and demonstrated that SWI could not only visually assess but also offered robust semi-quantitative measurement for IMH.

We evaluated the diagnostic performance of the three sequences and compared their image quality. Our study found that the imaging $rSNR_{IMH}$ of the T1 mapping was higher than that of SWI. However, SWI images had the highest CNR. The diagnostic performance showed no significant difference quantitatively or qualitatively among three imaging sequences. These findings could have been explained by two facts: the mapping technique has a relatively short scan time and uses motion correction, which can minimize artifacts; although SWI had a slightly longer

breath-holding time, it is sensitive to detection of the phase changes of small-sized structures (18). IMH with a small volume can be identified more easily on the SWI images compared to other two sequences, indicating that SWI is more sensitive to IMH detection. Moreover, the other advantage of SWI sequence is that it is a 3D image of the LV, whereas mapping sequence usually includes 11–13 slices of the LV. From this perspective, SWI is superior to T1 and T2 mapping in the extent of IMH detection. In our study, all the SWI images could be used to diagnose IMH, and the hypointense region was identifiable. SWI is susceptible to myocardial motion (29). To reduce this artifact during scanning, the phase encoding direction was set along the direction of infarcted myocardial contraction. Additionally, $SWI_{remote\text{-}infarct}$ showed excellent intra- and inter-observer consistency. These findings suggest that SWI is a feasible and reproducible imaging method for detecting IMH.

The median interval between the CMR examination time and PCI was 4 days in our study, similar to a previous study (10), However, this interval has been shorter or longer in other studies (26,30-32). Whether the interval impacts IMH detection and its prognostic value is unknown and needs to be studied in the future.

This study had several limitations. First, this was a preliminary study with a small sample size conducted in a single center. Future studies need to include a larger patient population. Secondly, there are artifacts on SWI images, which is largely due to the inability of ECG and respiratory gating to be performed on 3D sequences, and also, we did not quantify the IMH size, which was rarely related to the patient's prognosis as shown in a previous study (18), but further studies are warranted to investigate the potential value of the extent of IMH. Lastly, we did not have any data on the follow up of the patients; further follow up will be carried out in the future.

Conclusions

In conclusion, SWI, as well as T1/T2 mapping, is an accurate and reproducible approach for detecting IMH with excellent performance. When T2W-STIR images are unavailable, SWI may serve as an alternative.

Acknowledgments

Funding: This work was supported by grants from the National Natural Science Foundation of China (No. 81873889) and the Youth Fund of Hubei Science and Technology Plan (No. 2021CFB060).

Footnote

Reporting Checklist: The authors have completed the STARD reporting checklists. Available at https://qims.amegroups.com/article/view/10.21037/qims-23-591/rc

Conflicts of Interest: All authors have completed the ICMJE uniform disclosure form (available at https://qims.amegroups.com/article/view/10.21037/qims-23-591/coif). X.T. and X.Z. are current employees of Bayer Healthcare and Siemens Healthineers, respectively. The other authors have no conflicts of interest to declare.

Ethical Statement: The authors are accountable for all aspects of the work in ensuring that questions related to the accuracy or integrity of any part of the work are appropriately investigated and resolved. The study was conducted in accordance with the Declaration of Helsinki (as revised in 2013). The study was approved by the Ethics Committee of the Tongji's Hospital (No. [2019] S1184), and individual consent for this prospective analysis was obtained.

References

1. Steg PG, James SK, Atar D, Badano LP, Blömstrom-Lundqvist C, et al. ESC Guidelines for the management of acute myocardial infarction in patients presenting with ST-segment elevation. Eur Heart J 2012;33:2569-619.
2. Betgem RP, de Waard GA, Nijveldt R, Beek AM, Escaned J, van Royen N. Intramyocardial haemorrhage after acute myocardial infarction. Nat Rev Cardiol 2015;12:156-67.
3. Ghugre NR, Pop M, Thomas R, Newbigging S, Qi X, Barry J, Strauss BH, Wright GA. Hemorrhage promotes inflammation and myocardial damage following acute myocardial infarction: insights from a novel preclinical model and cardiovascular magnetic resonance. J Cardiovasc Magn Reson 2017;19:50.

4. Ferré-Vallverdú M, Sánchez-Lacuesta E, Plaza-López D, Díez-Gil JL, Sepúlveda-Sanchis P, Gil-Cayuela C, Maceira-Gonzalez A, Miró-Palau V, Montero-Argudo A, Martínez-Dolz L, Igual-Muñoz B. Prognostic value and clinical predictors of intramyocardial hemorrhage measured by CMR T2* sequences in STEMI. Int J Cardiovasc Imaging 2021;37:1735-44.
5. Ganame J, Messalli G, Dymarkowski S, Rademakers FE, Desmet W, Van de Werf F, Bogaert J. Impact of myocardial haemorrhage on left ventricular function and remodelling in patients with reperfused acute myocardial infarction. Eur Heart J 2009;30:1440-9.
6. Assimopoulos S, Shie N, Ramanan V, Qi X, Barry J, Strauss BH, Wright GA, Ghugre NR. Hemorrhage promotes chronic adverse remodeling in acute myocardial infarction: a T(1) , T(2) and BOLD study. NMR Biomed 2021;34:e4404.
7. Carrick D, Haig C, Ahmed N, McEntegart M, Petrie MC, Eteiba H, Hood S, Watkins S, Lindsay MM, Davie A, Mahrous A, Mordi I, Rauhalammi S, Sattar N, Welsh P, Radjenovic A, Ford I, Oldroyd KG, Berry C. Myocardial Hemorrhage After Acute Reperfused ST-Segment-Elevation Myocardial Infarction: Relation to Microvascular Obstruction and Prognostic Significance. Circ Cardiovasc Imaging 2016;9:e004148.
8. Driesen RB, Zalewski J, Vanden Driessche N, Vermeulen K, Bogaert J, Sipido KR, Van de Werf F, Claus P. Histological correlate of a cardiac magnetic resonance imaged microvascular obstruction in a porcine model of ischemia-reperfusion. Cardiovasc Pathol 2012;21:129-31.
9. Chen W, Zhang B, Xia R, Zhang R, Xu Z, Chen Y, Wang C, Wang L, Zheng J, Gao F. T2 mapping at 7T MRI can quantitatively assess intramyocardial hemorrhage in rats with acute reperfused myocardial infarction in vivo. J Magn Reson Imaging 2016;44:194-203.
10. Robbers LF, Eerenberg ES, Teunissen PF, Jansen MF, Hollander MR, Horrevoets AJ, Knaapen P, Nijveldt R, Heymans MW, Levi MM, van Rossum AC, Niessen HW, Marcu CB, Beek AM, van Royen N. Magnetic resonance imaging-defined areas of microvascular obstruction after acute myocardial infarction represent microvascular destruction and haemorrhage. Eur Heart J 2013;34:2346-53.
11. Stork A, Lund GK, Muellerleile K, Bansmann PM, Nolte-Ernsting C, Kemper J, Begemann PG, Adam G. Characterization of the peri-infarction zone using T2-weighted MRI and delayed-enhancement MRI in patients with acute myocardial infarction. Eur Radiol 2006;16:2350-7.
12. van den Bos EJ, Baks T, Moelker AD, Kerver W, van Geuns RJ, van der Giessen WJ, Duncker DJ, Wielopolski PA. Magnetic resonance imaging of haemorrhage within reperfused myocardial infarcts: possible interference with iron oxide-labelled cell tracking? Eur Heart J 2006;27:1620-6.
13. Zaman A, Higgins DM, Motwani M, Kidambi A, Kouwenhoven M, Kozerke S, Greenwood JP, Plein S. Robust myocardial T2 and T2 * mapping at 3T using image-based shimming. J Magn Reson Imaging 2015;41:1013-20.
14. Bulluck H, Rosmini S, Abdel-Gadir A, Bhuva AN, Treibel TA, Fontana M, Gonzalez-Lopez E, Ramlall M, Hamarneh A, Sirker A, Herrey AS, Manisty C, Yellon DM, Moon JC, Hausenloy DJ. Diagnostic performance of T(1) and T(2) mapping to detect intramyocardial hemorrhage in reperfused ST-segment elevation myocardial infarction (STEMI) patients. J Magn Reson Imaging 2017;46:877-86.
15. Ma YJ, Shao H, Fan S, Lu X, Du J, Young IR, Bydder GM. New options for increasing the sensitivity, specificity and scope of synergistic contrast magnetic resonance imaging (scMRI) using Multiplied, Added, Subtracted and/or FiTted (MASTIR) pulse sequences. Quant Imaging Med Surg 2020;10:2030-65.
16. Krishnan AS, Lansley JA, Jäger HR, Mankad K. New vistas in clinical practice: susceptibility-weighted imaging. Quant Imaging Med Surg 2015;5:448-52.
17. Durighel G, Tokarczuk PF, Karsa A, Gordon F, Cook SA, O'Regan DP. Acute myocardial infarction: susceptibility-weighted cardiac MRI for the detection of reperfusion haemorrhage at 1.5 T. Clin Radiol 2016;71:e150-6.
18. Kidambi A, Biglands JD, Higgins DM, Ripley DP, Zaman A, Broadbent DA, McDiarmid AK, Swoboda PP, Al Musa T, Erhayiem B, Greenwood JP, Plein S. Susceptibility-weighted cardiovascular magnetic resonance in comparison to T2 and T2 star imaging for detection of intramyocardial hemorrhage following acute myocardial infarction at 3 Tesla. J Cardiovasc Magn Reson 2014;16:86.
19. Yancy CW, Jessup M, Bozkurt B, Butler J, Casey DE Jr, Drazner MH, et al. 2013 ACCF/AHA guideline for the management of heart failure: a report of the American College of Cardiology Foundation/American Heart Association Task Force on Practice Guidelines. J Am Coll Cardiol 2013;62:e147-239.
20. Kellman P, Hansen MS. T1-mapping in the heart: accuracy and precision. J Cardiovasc Magn Reson 2014;16:2.

21. Bondarenko O, Beek AM, Hofman MB, Kühl HP, Twisk JW, van Dockum WG, Visser CA, van Rossum AC. Standardizing the definition of hyperenhancement in the quantitative assessment of infarct size and myocardial viability using delayed contrast-enhanced CMR. J Cardiovasc Magn Reson 2005;7:481-5.
22. Goldfarb JW, Hasan U, Zhao W, Han J. Magnetic resonance susceptibility weighted phase imaging for the assessment of reperfusion intramyocardial hemorrhage. Magn Reson Med 2014;71:1210-20.
23. DeLong ER, DeLong DM, Clarke-Pearson DL. Comparing the areas under two or more correlated receiver operating characteristic curves: a nonparametric approach. Biometrics 1988;44:837-45.
24. Ghugre NR, Ramanan V, Pop M, Yang Y, Barry J, Qiang B, Connelly KA, Dick AJ, Wright GA. Quantitative tracking of edema, hemorrhage, and microvascular obstruction in subacute myocardial infarction in a porcine model by MRI. Magn Reson Med 2011;66:1129-41.
25. Guo H, Au WY, Cheung JS, Kim D, Jensen JH, Khong PL, Chan Q, Chan KC, Tosti C, Tang H, Brown TR, Lam WW, Ha SY, Brittenham GM, Wu EX. Myocardial T2 quantitation in patients with iron overload at 3 Tesla. J Magn Reson Imaging 2009;30:394-400.
26. Kali A, Tang RL, Kumar A, Min JK, Dharmakumar R. Detection of acute reperfusion myocardial hemorrhage with cardiac MR imaging: T2 versus T2. Radiology 2013;269:387-95.
27. Wu KC. CMR of microvascular obstruction and hemorrhage in myocardial infarction. J Cardiovasc Magn Reson 2012;14:68.
28. Blondiaux E, Pidial L, Vilar J, Autret G, Balvay D, Audureau E, Bruneval P, Bel A, Cuenod CA, Silvestre JS, Clément O. Evaluation of rat heart microvasculature with high-spatial-resolution susceptibility-weighted MR imaging. Radiology 2013;269:277-82.
29. Goldfarb JW, Hasan U. Imaging of reperfused intramyocardial hemorrhage with cardiovascular magnetic resonance susceptibility weighted imaging (SWI). PLoS One 2015;10:e0123560.
30. O'Regan DP, Ahmed R, Karunanithy N, Neuwirth C, Tan Y, Durighel G, Hajnal JV, Nadra I, Corbett SJ, Cook SA. Reperfusion hemorrhage following acute myocardial infarction: assessment with T2* mapping and effect on measuring the area at risk. Radiology 2009;250:916-22.
31. van Kranenburg M, Magro M, Thiele H, de Waha S, Eitel I, Cochet A, Cottin Y, Atar D, Buser P, Wu E, Lee D, Bodi V, Klug G, Metzler B, Delewi R, Bernhardt P, Rottbauer W, Boersma E, Zijlstra F, van Geuns RJ. Prognostic value of microvascular obstruction and infarct size, as measured by CMR in STEMI patients. JACC Cardiovasc Imaging 2014;7:930-9.
32. Zia MI, Ghugre NR, Connelly KA, Strauss BH, Sparkes JD, Dick AJ, Wright GA. Characterizing myocardial edema and hemorrhage using quantitative T2 and T2* mapping at multiple time intervals post ST-segment elevation myocardial infarction. Circ Cardiovasc Imaging 2012;5:566-72.

Cite this article as: Wen J, Qiao J, Tang Y, Zhao Y, Yang Z, Wang L, Tao X, Zhou X, Xia L, Tang D, Huang L. Cardiac magnetic resonance imaging detection of intramyocardial hemorrhage in patients with ST-elevated myocardial infarction: comparison between susceptibility-weighted imaging and T1/T2 mapping techniques. Quant Imaging Med Surg 2024;14(1):476-488. doi: 10.21037/qims-23-591

Supplementary

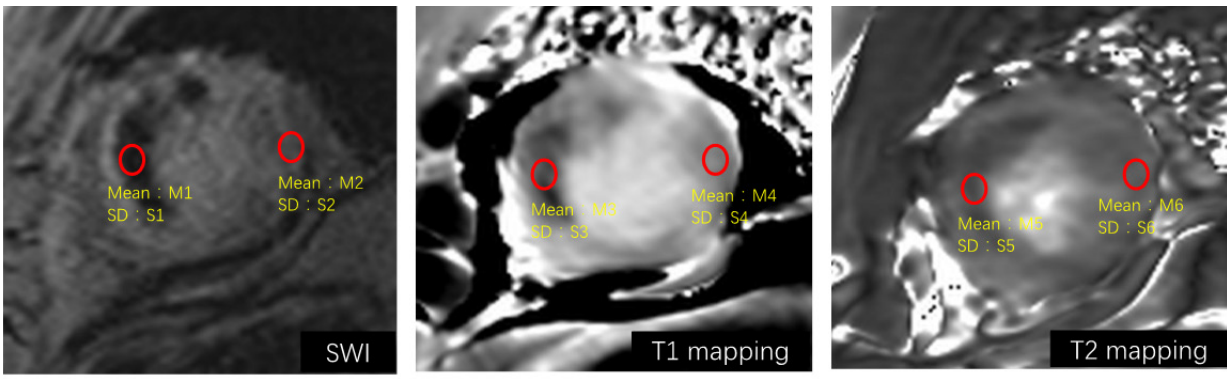

$$\mathrm{rSNR_{IMH}} = 0.655\times\frac{M1}{S1} \qquad \mathrm{rSNR_{IMH}} = 0.655\times\frac{M2}{S2} \qquad \mathrm{rSNR_{IMH}} = 0.655\times\frac{M3}{S3}$$

$$CNR = \frac{|M2 - M1|}{S2} \qquad CNR = \frac{|M4 - M3|}{S4} \qquad CNR = \frac{|M6 - M5|}{S6}$$

Figure S1 The measurement of rSNRIMH and CNR on three MRI sequences. SD, standard deviation; SWI, susceptibility-weighted imaging; rSNRIMH, relative signal intensity-to-noise ratios within IMH area; IMH, intramyocardial hemorrhage; CNR, contrast-to-noise ratio; MRI, magnetic resonance imaging.

Table S1 The cross tabulation of diagnostic results of the reference standard and three sequences

Variables	Clinical diagnose		Total	Fisher P value
	With IMH	Without IMH		
T1 mapping				<0.001
$T1_{infarct\text{-}remote}$ <1.100	26	2	28	
$T1_{infarct\text{-}remote}$ ≥1.100	0	8	8	
Total	26	10	36	
T2 mapping				<0.001
$T2_{infarct\text{-}remote}$ <0.893	24	0	24	
$T2_{infarct\text{-}remote}$ ≥0.893	2	10	12	
Total	26	10	36	
SWI				<0.001
$SWI_{infarct\text{-}remote}$ <0.891	26	0	26	
$SWI_{infarct\text{-}remote}$ ≥0.891	0	10	10	
Total	26	10	36	

IMH, intramyocardial hemorrhage; SWI, susceptibility-weighted imaging.

https://dx.doi.org/10.21037/qims-23-591

Table S2 Intraobserver and interobserver variability

Variables	Intraobserver			Interobserver		
	ICC	Cohen's kappa	95% CI	ICC	Cohen's kappa	95% CI
$T1_{infarct\text{-}remote}$	0.96		0.92–0.98	0.96		0.92–0.98
$T2_{infarct\text{-}remote}$	0.81		0.66–0.90	0.89		0.79–0.94
$SWI_{infarct\text{-}remote}$	0.92		0.84–0.96	0.90		0.82–0.95
Sequences						
T1 mapping		0.83	0.94–1.00		0.83	0.65–1.00
T2 mapping		0.82	0.64–1.00		0.88	0.73–1.00
SWI		0.88	0.71–1.00		0.88	0.72–1.00

ICC, intraclass correlation coefficient; CI, confidence intervals; SWI, susceptibility-weighted imaging.

https://dx.doi.org/10.21037/qims-23-591